Spectral Efficiency of MIMO Millimeter-Wave Links with Single-Carrier Modulation for 5G Networks

Stefano Buzzi, Carmen D'Andrea
DIEI - Università di Cassino
e del Lazio Meridionale
I-03043 Cassino (FR) - Italy

Tommaso Foggi, Alessandro Ugolini,
Giulio Colavolpe
DII - Università di Parma
I-43124, Parma - Italy

***Abstract*—Future wireless networks will extensively rely upon bandwidths centered on carrier frequencies larger than 10GHz. Indeed, recent research has shown that, despite the large path-loss, millimeter wave (mmWave) frequencies can be successfully exploited to transmit very large data-rates over short distances to slowly moving users. Due to hardware complexity and cost constraints, single-carrier modulation schemes, as opposed to the popular multi-carrier schemes, are being considered for use at mmWave frequencies. This paper presents preliminary studies on the achievable spectral efficiency on a wireless MIMO link operating at mmWave in a typical 5G scenario. Two different single-carrier modulations are considered, i.e. a traditional modulation scheme with linear equalization at the receiver, and a single-carrier modulation with cyclic prefix, frequency-domain equalization and FFT-based processing at the receiver. Our results, obtained with reference to different shaping pulses, show that both schemes attain good performance levels, although the former achieves a larger spectral efficiency than the latter. Results also confirm that the spectral efficiency increases with the dimension of the antenna array, as well as that performance gets severely degraded when the link length exceeds 90-100 meters and the transmit power falls below 0dBW.**

I. Introduction

The research on the next generation of wireless networks is proceeding at an intense pace, both in industry and in academia. Focusing on the Physical Layer, there is wide agreement [1] that fifth-generation (5G) wireless networks will be based, among the others, on three main innovations with respect to legacy fourth-generation systems, and in particular (a) the use of large scale antenna arrays, a.k.a. massive MIMO [2]; (b) the use of small-size cells in areas with very large data request [3]; and (c) the use of carrier frequencies larger than 10GHz [4].

Indeed, focusing on (c), the use of the so-called millimeter wave (mmWave) frequencies has been proposed as a strong candidate approach to achieve the spectral efficiency growth required by 5G wireless networks, resorting to the use of currently unused frequency bands in the range between 20 GHz and 90 GHz. In particular, the E-band between 70 GHz and 80 GHz provides 10 GHz of free spectrum which could be exploited to operate 5G networks. It is worth underlining that mmWave are not intended to replace the use of lower carrier frequencies traditionally used for cellular communications, but rather as additional frequencies that can be used in densely crowded areas for short-range communications. Until now, the use of mmWave for cellular communications has been neglected due to the higher atmospheric absorption that they suffer compared to other frequency bands and to the larger values of the free-space path-loss. However, recent measurements suggest that mmWave attenuation is only slightly worse than in other bands, as far as propagation in dense urban environments and over short distances (up to about 100 meters) is concerned [5]. Additionally, since antennas at these wavelengths are very small, arrays with several elements can be packed in small volumes, in principle also on mobile devices, thus removing the traditional constraint that only few antennas can be placed on a smartphone and benefiting of a doubled array gain with respect to traditional cellular links. Another peculiar feature of cellular communications at mmWave that has been found is that these are mainly noise-limited and not interference-limited systems, and this will simplify the implementation of interference-management and resource-scheduling policies. Based on this encouraging premises, a large body of work has been recently carried out on the use of mmWave for cellular communications [4], [5], [6], [7], [8].

One of the key questions about the use of mmWave is about the type of modulation that will be used at these frequencies. Indeed, while it is not even sure that 5G systems will use orthogonal frequency division multiplexing (OFDM) modulation at classical cellular frequencies [9], there are several reasons that push for 5G networks operating a single-carrier modulation (SCM) at mmWave [5]. First of all, the propagation attenuation of mmWave make them a viable technology only for small-cell, dense networks, where few users will be associated to any given base station, thus implying that the efficient frequency-multiplexing features of OFDM may not be really needed. Additionally, the large bandwidth would cause low OFDM symbol duration, which, coupled with small propagation delays, means that the users may be multiplexed in the time domain as efficiently as in the frequency domain. Finally, mmWave will be operated together with massive antenna arrays to overcome propagation

attenuation. This makes digital beamforming unfeasible, since the energy required for digital-to-analog and analog-to-digital conversion would be huge. Thus, each user will have an own radio-frequency beamforming, which requires users to be separated in time rather than frequency.

In light of these considerations, SCM formats are being seriously considered for mmWave systems. For efficient removal of the intersymbol interference induced by the frequency-selective nature of the channel, the use of SCM coupled with a cyclic prefix has been proposed, so that FFT-based processing might be performed at the receiver [10] In [11], [12], the null cyclic prefix single carrier (NCP-SC) scheme has been proposed for mmWave. The concept is to transmit a single-carrier signal, in which the usual cyclic prefix used by OFDM is replaced by nulls appended at the end of each transmit symbol. The block scheme is reported in Fig. 1.

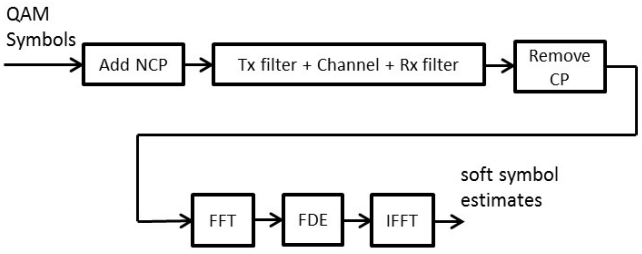

Fig. 1. Principle of NCP-SCM transceiver architecture; FDE stands for "frequency-domain equalization".

This paper is concerned with the evaluation of the achievable spectral efficiency (ASE) of SCM schemes operating over MIMO links at mmWave frequencies. We consider two possible transceiver architectures: (a) SCM with linear minimum mean square error (LMMSE) equalization in the time domain for intersymbol interference removal and symbol-by-symbol detection; and (b) SCM with cyclic prefix and FFT-based processing and LMMSE equalization in the frequency domain at the receiver. By adopting, inspired by [13], [14], a modified statistical MIMO channel model for mmWave frequencies, and using the simulation-based technique for computing information-rates reported in [15], we thus provide a preliminary assessment of the achievable spectral efficiency (ASE) that can be reasonably expected in a scenario representative of a 5G environment, studying also the impact of different pulse-shaping filters at the transmitter and at the receiver. Our results show that, for distances less than 100 meters, and with a transmit power around 0dBW, mmWave links exhibit good performance and may provide spectral efficiency quite close to the theoretical maximum values; for larger distances instead, either large values of the transmit power or a large number of antennas must be employed to overcome the distance-dependent increased attenuation.

The rest of this paper is organized as follows. Next Section contains the system model, with details on the two considered transceiver architectures and on the pulse shapes considered in the paper. Section III explains the used technique for the evaluation of the ASE, while extensive numerical results are illustrated and discussed in Section IV. Finally, Section V contains concluding remarks.

II. System model

We consider a transmitter-receiver pair that may be representative of either the uplink or the downlink of a cellular system. We denote by N_T and N_R the number of transmit and receive antennas, respectively. Denote by $\mathbf{s}$ a column vector containing the L data-symbols (drawn from a QAM constellation with average energy P_T) to be transmitted:

$$\mathbf{s} = [s_0, s_1, \ldots, s_{L-1}]^T \ , \tag{1}$$

with $(\cdot)^T$ denoting transpose. We assume that $L = kM$, where k is an integer and M is the number of information symbols that are simultaneously transmitted by the N_T transmit antennas in each symbol interval. The propagation channel is modeled in discrete-time as a matrix-valued finite-impulse-response (FIR) filter; in particular, we denote by $\{\mathbf{H}(n)\}_{n=0}^{P-1}$ the sequence, of length P, of the $(N_R \times N_T)$-dimensional matrices describing the channel. The discrete-time versions of the impulse response of the transmit and receive shaping filters are denoted as $h_{TX}(n)$ and $h_{RX}(n)$, respectively; these filters are assumed to be both of length P_h.

We focus on two different transceiver architectures, one that operates equalization in the time-domain and one that works in the frequency domain through the use of a cyclic prefix.

A. Transceiver model with time-domain equalization (TDE)

We refer to the discrete-time block-scheme reported in Fig. 2. The QAM symbols in the vector $\mathbf{s}$ are fed to a serial-to-parallel conversion block that splits them in k distinct M-dimensional vectors $\check{\mathbf{s}}(1), \ldots, \check{\mathbf{s}}(k)$. These vectors are precoded using the the $(N_T \times M)$-dimensional precoding matrix $\mathbf{Q}$; we thus obtain the N_T-dimensional vectors

$$\mathbf{x}(n) = \mathbf{Q}\check{\mathbf{s}}(n) \ , \qquad n = 1, \ldots, k \ .$$

The vectors $\mathbf{x}(n)$ are fed to a bank of N_T identical shaping filters, converted to RF and transmitted.

At the receiver, after baseband-conversion, the N_R received signals are passed through a bank of filters matched to the ones used for transmission and sampled at symbol-rate. We thus obtain the N_R-dimensional vectors $\mathbf{y}(n)$, which are passed through a post-coding matrix, that we denote by $\mathbf{D}$, of dimension $(N_R \times M)$. Denoting by $\widetilde{\mathbf{H}}(n)$ the matrix-valued FIR filter representing the composite channel impulse response (i.e., the convolution of the transmit filter, actual matrix-valued channel and receive filter), it is easy to show that the generic M-dimensional vector at the output of the post-coding matrix, say $\widetilde{\mathbf{r}}(n)$, is written as

$$\widetilde{\mathbf{r}}(n) = \mathbf{D}^H\mathbf{y}(n) = \sum_{\ell=0}^{\widetilde{P}-1} \mathbf{D}^H\widetilde{\mathbf{H}}(\ell)\mathbf{Q}\check{\mathbf{s}}(n-\ell) + \mathbf{D}^H\mathbf{w}(n) \ , \tag{2}$$

with $(\cdot)^H$ denoting conjugate transpose. In (2), $\widetilde{P} = P + 2P_h - 1$ is the length of the matrix-valued composite channel

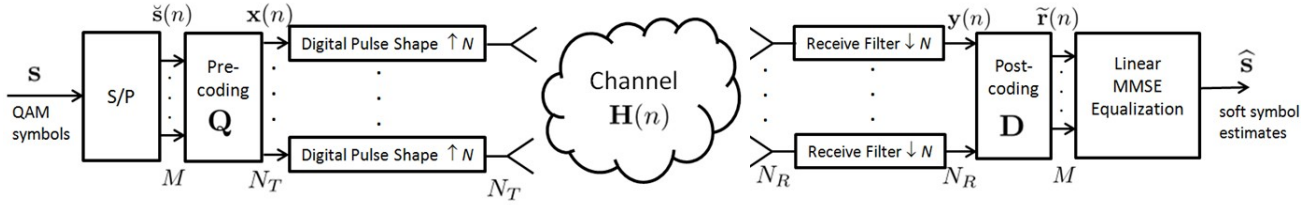

Fig. 2. Transceiver architecture with time-domain equalization.

impulse response $\widetilde{\mathbf{H}}(n)$, while $\mathbf{w}(n)$ is the additive Gaussian-distributed thermal noise at the output of the reception filter. In order to combat the intersymbol interference, an LMMSE equalizer is used. In particular, to obtain a soft estimate of the data vector $\check{\mathbf{s}}(n)$, the $Q+1$ observables $\widetilde{\mathbf{r}}(n-Q/2), \widetilde{\mathbf{r}}(n-Q/2+1), \ldots, \widetilde{\mathbf{r}}(n+Q/2)$ are stacked into a single $(Q+1)M$-dimensional vector, that we denote by $\widetilde{\mathbf{r}}_{Q+1}(n)$, and processed as follows:

$$\widehat{\check{\mathbf{s}}}(n) = \mathbf{E}^H \widetilde{\mathbf{r}}_{Q+1}(n) \,, \tag{3}$$

where $\mathbf{E}$ is a $[(Q+1)M \times M]$-dimensional matrix representing the LMMSE equalizer[1].

B. Transceiver model with frequency-domain equalization (FDE)

We refer to the discrete-time block-scheme reported in Fig. 3. A CP of length CM is added at the beginning of the block $\mathbf{s}$ of $L = kM$ QAM symbols, so as to have the vector $\widetilde{\mathbf{s}}$ of lenght $(k+C)M$. As in the previous case, the vector $\widetilde{\mathbf{s}}$ is passed through a serial-to-parallel conversion with M outputs, a precoding block (again expressed through the matrix $\mathbf{Q}$), a bank of N_T transmit filters; then conversion to RF and transmission take place. At the receiver, after baseband-conversion, the N_R received signals are passed through a bank of filters matched to the ones used for transmission and sampled at symbol-rate; then, the cyclic prefix is removed. We thus obtain the N_R-dimensional vectors $\mathbf{y}^{\mathrm{CP}}(n)$, with $n = 1, \ldots, k$, containing a noisy version of the *circular* convolution between the sequence $\mathbf{x}^{\mathrm{CP}}(n)$ and $\widetilde{\mathbf{H}}(n)$, i.e.:

$$\mathbf{y}^{\mathrm{CP}}(n) = \widetilde{\mathbf{H}}(n) \circledast \mathbf{x}^{\mathrm{CP}}(n) + \mathbf{w}(n) \,, \qquad n = 1, \ldots, k \tag{4}$$

The vectors $\mathbf{y}^{\mathrm{CP}}(n)$ then go through an entry-wise FFT transformation on k points; the n-th FFT coefficient, with $n = 1, \ldots, k$, can be shown to be expressed as

$$\mathbf{Y}^{\mathrm{CP}}(n) = \widetilde{\mathcal{H}}(n) \mathbf{X}^{\mathrm{CP}}(n) + \mathbf{W}(n) \,, \tag{5}$$

where $\widetilde{\mathcal{H}}(n)$ is an $(N_R \times N_T)$-dimensional matrix representing the n-th FFT coefficient of the matrix-valued sequence $\widetilde{\mathbf{H}}(n)$, and $\mathbf{X}^{\mathrm{CP}}(n)$ and $\mathbf{W}(n)$ are the n-th FFT coefficient of the sequences $\mathbf{x}^{\mathrm{CP}}(n)$ and $\mathbf{w}(n)$, respectively. From Eq. (5) it is seen that, due to the presence of multiple antennas, and, thus, of the matrix-valued channel, the useful symbols reciprocally interfere and thus an equalizer is needed. We denote by $\mathbf{E}(n)$ the $(N_T \times N_R)$-dimensional matrix equalization matrix such that

$$\mathbf{Z}^{\mathrm{CP}}(n) = \mathbf{E}^H(n) \mathbf{Y}^{\mathrm{CP}}(n)$$

provides an LMMSE estimate of the vector $\mathbf{X}^{\mathrm{CP}}(n)$. Then, the vectors $\mathbf{Z}^{\mathrm{CP}}(n)$ go through an entry-wise IFFT transformation on k points, and, finally, a postcoding block yields the soft symbol estimates of the entries of the data vector $\mathbf{s}$.

[1]We do not report here its explicit expression for the sake of brevity.

C. Waveform choice

In this section, we describe some shaping pulses that are currently being considered as alternatives to the rectangular pulse adopted in OFDM and that can be used also as shaping transmit and receive filters in our considered modulation schemes. In practice, we are interested in pulses that achieve a good compromise between their sidelobe levels in the frequency domain, and their extension in the time-domain. We consider three possible examples of pulse shapes, namely the evergreen root-raised cosine (RRC), the pulse proposed in the PHYDYAS research project [16] for use with the Filterbank Multi-Carrier modulation, and, finally, the Dolph-Chebyshev (DC) pulse.

RRC pulses are widely used in telecommunication systems to minimized ISI at the receiver. The impulse response of an RRC pulse is

$$p(t) = \begin{cases} \frac{1}{\sqrt{T}} \left(1 - \alpha + 4\frac{\alpha}{\pi}\right) & t = 0 \\ \frac{\alpha}{\sqrt{2T}} \left[\left(1 + \frac{2}{\pi}\right) \sin\left(\frac{\pi}{4\alpha}\right) + \left(1 - \frac{2}{\pi}\right) \cos\left(\frac{\pi}{4\alpha}\right)\right] & t = \pm\frac{T}{4\alpha} \\ \frac{1}{\sqrt{T}} \frac{\sin\left(\pi \frac{t}{T}(1-\alpha)\right) + 4\alpha \frac{t}{T} \cos\left(\pi \frac{t}{T}(1+\alpha)\right)}{\pi \frac{t}{T}\left[1 - \left(4\alpha \frac{t}{T}\right)^2\right]} & \text{otherwise} \end{cases} \tag{6}$$

where T is the symbol interval and α is the roll-off factor, which measures the excess bandwidth of the pulse in the frequency domain.

The PHYDYAS pulse is a discrete-time pulse specifically designed for FBMC systems. Let M be the number of sub-carriers, then the impulse response is

$$p(n) = P_0 + 2 \sum_{k=1}^{K-1} (-1)^k P_k \cos\left(\frac{2\pi k}{KM}(n+1)\right) \,,$$

for $n = 0, 1, \ldots, KM-2$ and $K = 4$, where the coefficients $P_k,\ k = 0, \ldots, K-1$ have been selected using the frequency

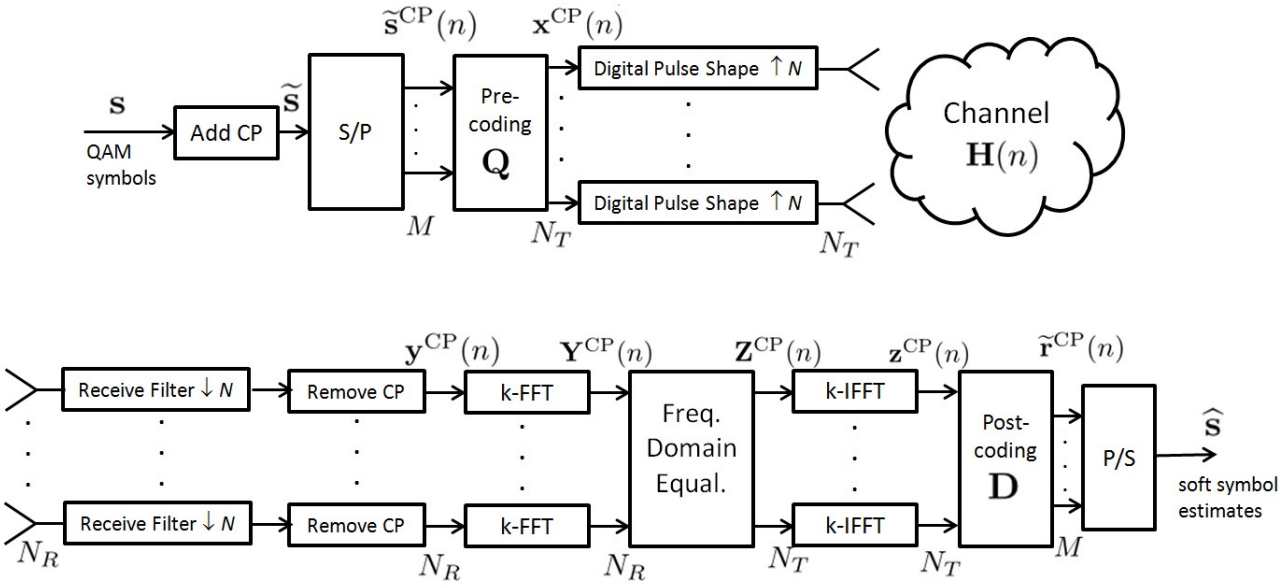

Fig. 3. transceiver architecture with cyclic prefix, FFT-based processing and frequency-domain equalization.

sampling technique [16], and assume the following values:

$$\begin{aligned} P_0 &= 1 \\ P_1 &= 0.97195983 \\ P_2 &= 1/\sqrt{2} \\ P_3 &= \sqrt{1-P[1]}\,. \end{aligned}$$

The DC pulse [17] is significant because, in the frequency domain, it minimizes the main lobe width for a given side lobe attenuation. Its discrete-time impulse response is [18]

$$p(n) = \tfrac{1}{N}\left[10^{-\frac{A}{20}} + 2\sum_{k=1}^{(N-1)/2} T_{N-1}\left(x_0 \cos\left(\tfrac{k\pi}{N}\right)\right)\cos\left(\tfrac{2\pi n k}{N}\right)\right],$$

for $n = 0, \pm 1, \ldots, \pm\frac{N-1}{2}$, where N is the number of coefficients, A is the attenuation of side lobes in dB,

$$x_0 = \cosh\left(\frac{1}{N-1}\cosh^{-1}\left(10^{-\frac{A}{20}}\right)\right),$$

and

$$T_n(x) = \begin{cases} \cos\left(n\cos^{-1}(x)\right) & |x| \le 1 \\ \cosh\left(n\cosh^{-1}(x)\right) & |x| > 1 \end{cases}$$

is the Chebyshev polynomial of the first kind [19].

In Fig. 4, we report the spectra of the pulses we have just described. All spectra were computed by performing a 1024 points FFT of pulses of 160 samples in the time domain. The figure compares the rectangular pulse, typical of OFDM, with an RRC pulse having roll-off $\alpha = 0.1$, the PHYDYAS pulse with $M = 1$, and the DC pulse with attenuation $A = -50$ dB. The figure clearly shows that the rectangular pulse is the one with the worst spectral characteristics; on the other hand, the PHYDYAS pulse is the one with the smallest sidelobe levels, while the DC pulse is the one with the smallest width of the main lobe.

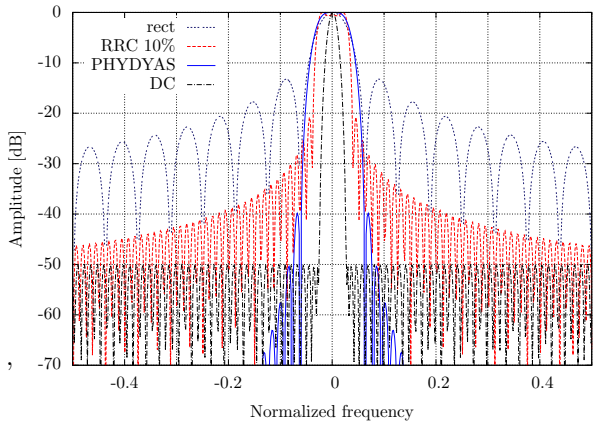

Fig. 4. Comparison of pulse shapes in the frequency domain.

III. Computation of the achievable spectral efficiency

In both transceiver models described in Section II the soft symbol estimates can be expressed in the form

$$\widehat{\mathbf{s}}(n) = \mathbf{A}\mathbf{s}(n) + \sum_{\ell \neq 0} \mathbf{A}_\ell \mathbf{s}(n-\ell) + \mathbf{z}(n)$$

i.e., as a linear transformation (through matrix $\mathbf{A}$) of the desired QAM data symbols, plus a linear combination of the interfering data symbols and the colored noise $\mathbf{z}(n)$ having a proper covariance matrix.

As a figure of merit to compare the different transceiver architectures with the different employed pulses, we will use the ASE, that is the maximum attainable spectral efficiency with the constraint of arbitrarily small BER. For notational simplicity, we omit the dependence of ASE on the SNR. The

ASE takes the particular constellation and signaling parameters into consideration, so it does not qualify as a normalized capacity measure (it is often called *constrained capacity*). We evaluate only ergodic rates so the ASE is computed given the channel realization and averaged over it—remember that we are assuming perfect channel state information at the receiver. The spectral efficiency of any practical coded modulation system operating at a low packet error rate is upper bounded by the ASE, i.e., $\rho \leq \text{ASE}$, where

$$\text{ASE} = \frac{1}{T_s W} \lim_{L\to\infty} \frac{1}{L} E_{\tilde{\mathbf{H}}} \left[I(\mathbf{s}; \hat{\mathbf{s}} | \tilde{\mathbf{H}}) \right] \text{ bit/s/Hz} \qquad (7)$$

$I(\mathbf{s}; \hat{\mathbf{s}}|\tilde{\mathbf{H}})$ being the mutual information given the channel realization, T_s the symbol interval, and W the signal bandwidth (as specified in Section IV).

The computation of the mutual information requires the knowledge of the channel conditional probability density function (pdf) $p(\hat{\mathbf{s}}|\mathbf{s}, \tilde{\mathbf{H}})$. In addition, only the optimal detector for the actual channel is able to achieve the ASE in (7). We are instead interested in the achievable performance when using suboptimal low-complexity detectors. For this reason, we resort to the framework described in [15, Section VI]. We compute proper lower bounds on the mutual information (and thus on the ASE) obtained by substituting $p(\hat{\mathbf{s}}|\mathbf{s}, \tilde{\mathbf{H}})$ in the mutual information definition with an arbitrary auxiliary channel law $q(\hat{\mathbf{s}}|\mathbf{s}, \tilde{\mathbf{H}})$ with the same input and output alphabets as the original channel (mismatched detection [15]). If the auxiliary channel law can be represented/described as a finite-state channel, the pdfs $q(\hat{\mathbf{s}}|\mathbf{s}, \tilde{\mathbf{H}})$ and $q_p(\hat{\mathbf{s}}|\tilde{\mathbf{H}}) = \sum_{\mathbf{s}} q(\hat{\mathbf{s}}|\mathbf{s}, \tilde{\mathbf{H}}) P(\mathbf{s})$ can be computed, this time, by using the optimal maximum a posteriori symbol detector for that auxiliary channel [15]. This detector, that is clearly suboptimal for the actual channel, has at its input the sequence $\hat{\mathbf{s}}$ generated by simulation *according to the actual channel model* [15]. If we change the adopted receiver (or, equivalently, if we change the auxiliary channel) we obtain different lower bounds on the constrained capacity but, in any case, these bounds are *achievable* by those receivers, according to mismatched detection theory [15]. We thus say, with a slight abuse of terminology, that the computed lower bounds are the ASE values of the considered channel when those receivers are employed.

This technique thus allows us to take reduced complexity receivers into account. In fact, it is sufficient to consider an auxiliary channel which is a simplified version of the actual channel in the sense that only a portion of the actual channel memory and/or a limited number of impairments are present.

In particular, in this paper we only consider auxiliary channel laws of the form

$$q(\hat{\mathbf{s}}|\mathbf{s}, \tilde{\mathbf{H}}) = \prod_n q[\hat{\mathbf{s}}(n)|\mathbf{s}(n), \tilde{\mathbf{H}}] \qquad (8)$$

i.e., the processing is made on each vector $\hat{\mathbf{s}}(n)$ independently and is also assumed that the interference is assimilated to Gaussian noise.

The transceiver models with the different shaping pulses are compared in terms of ASE without taking into account specific coding schemes, being understood that, with a properly designed channel code, the information-theoretic performance can be closely approached.

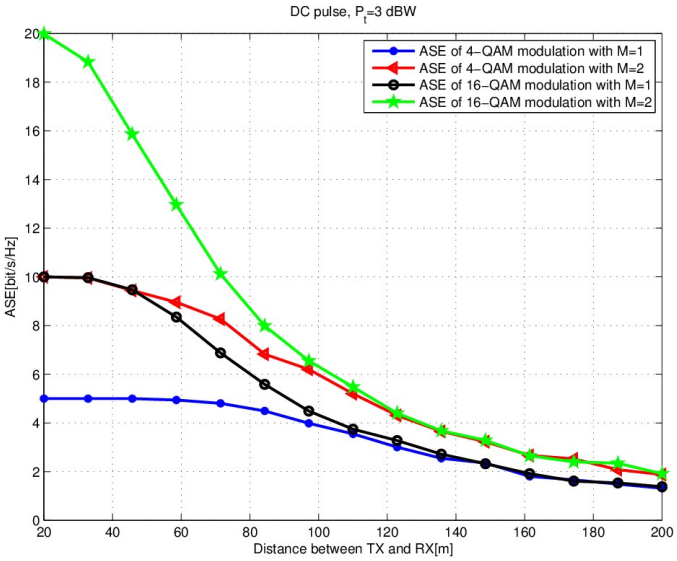

Fig. 5. ASE versus distance; impact of modulation cardinality and multiplexing order.

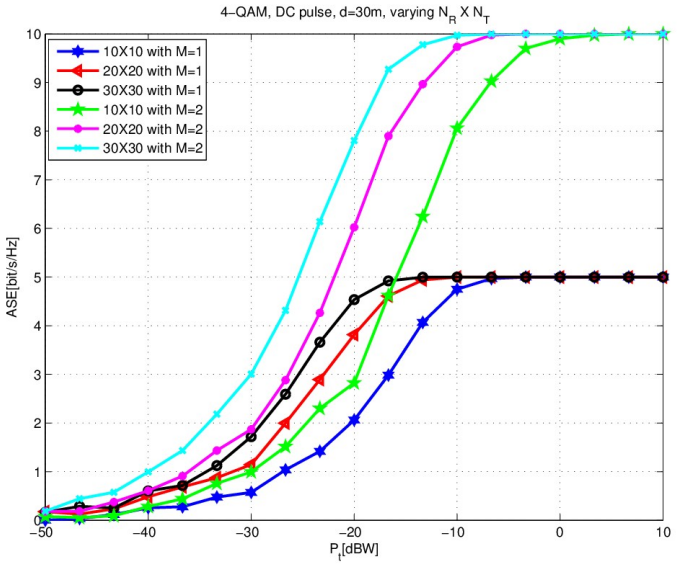

Fig. 6. ASE versus transmit power; impact of array size and multiplexing order.

IV. Numerical Results

We now report some simulation results. We consider a communication bandwidth of $W = 500$MHz centered over a mmWave carrier frequency. The MIMO propagation channel has been generated according to the statistical procedure detailed in [13], [14], with a path-loss exponent equal to 3.3 [20]. The additive thermal noise is assumed to have a power spectral density of -174dBm/Hz, while the front-end receiver is assumed to have a noise figure of 3dB. We study, in the

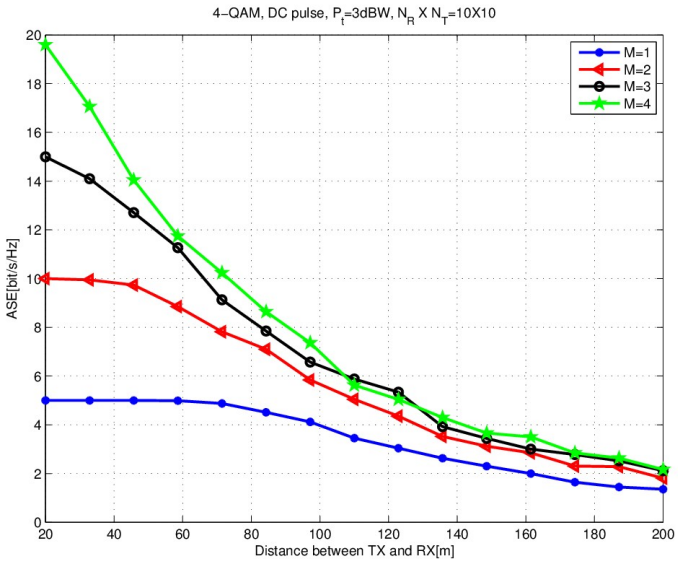

Fig. 7. ASE versus distance; impact of multiplexing order.

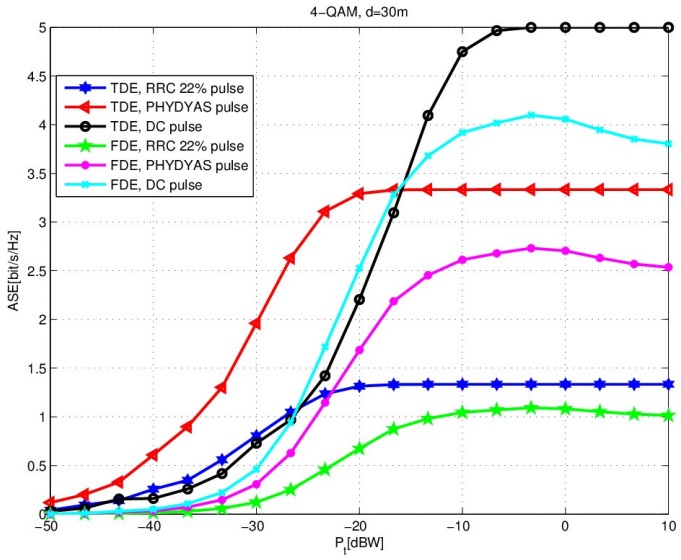

Fig. 8. ASE versus transmit power; comparison of TDE and FDE and impact of pulse shapes.

following figures, the ASE for varying values of the transmit power P_t, of the distance d between the transmitter and the receiver, of the number of transmit and receive antennas, of the multiplexing order M, and for the RRC pulse shape with 22% roll-off, the DC pulse, and the PHYDYAS pulse. For each waveform, we define the bandwidth as the frequency range such that out-of-band emissions are 40dB below the maximum in-band value of the Fourier transform of the pulse. This implies that the three considered pulses have different normalized bandwidths and, thus, their adoption results in different values of the symbol interval. For the considered communication bandwidth of $W = 500$MHz, we found that the symbol interval T_s is 3ns for the RRC pulse, 1.2ns for the PHYDYAS pulse, and 0.8ns for the DC pulse. The reported results are to be considered as ideal benchmark for the ASE since we are neglecting the interference[2], and we are considering digital pre-coding and post-coding, whereas due to hardware constraints mmWave systems will likely operate with hybrid analog/digital beamforming strategies [8][3]. Fig.s 5, 7 and 9 report the ASE[4] versus the distance d between the transmitter and the receiver (varying in the range $[20, 200]$m), assuming that the transmit power is $P_t = 3$dBW, while Fig.s 6 and 8 report the ASE versus the transmit power P_t (varying in the range $[-50, 10]$dBW), assuming a link length $d = 30$ m. Fig. 8 contains a comparison between the TDE and FDE transceiver architectures, while the remaining figures refer to the TDE transceiver structure. The LMMSE equalizer in the TDE structure spans a number of symbol intervals (that we have denoted as $Q + 1$) equal to the length $\widetilde{P}$ of the composite propagation channel. Inspecting the figures, the following remarks are in order:

- The proposed transceiver architecture with TDE outperforms the one with FDE. This result can be simply explained since the TDE equalizer makes a block-processing of the observables and has a larger computational complexity with respect to the FDE stucture.
- Among the considered pulse waveforms, the DC pulse achieves the best performance, in the light of its narrower main lobe.
- Results, in general, improve for increasing transmit power, for decreasing distance d between transmitter and receiver and for increasing values of the number of transmit and receive antennas.
- In particular, good performance can be attained for distances up to 100m, whereas for $d > 100m$ we have a steep degradation of the ASE. In this region, all the advantages given by increasing the modulation cardinality or the number of antennas are essentially lost or reduced at very small values.
- For a reference distance of 30m (which will be a typical one in small-cell 5G deployments for densely crowded areas), a trasnmit power around 0dBW is enough to grant good performance and to benefit from the advantages of increased modulation cardinality, size of the antenna array, and multiplexing order.

V. Conclusion

This paper has provided a preliminary assessment of the ASE for a MIMO link operating at mmWave frequencies with SCM. Two different transceiver architectures have been

[2]We note however that being mmWave systems mainly noise-limited rather than interference limited, the impact of this assumption on the obtained results is very limited.

[3]The evaluation of the ASE with hybrid analog/digital pre-coding and post-coding structures is an interesting issue that is out of the scope of this paper but certainly worth future investigation.

[4]Of course, the achievable rates in bit/s can be immediately obtained by multiplying the ASE by the communication bandwidth $W = 500$MHz.

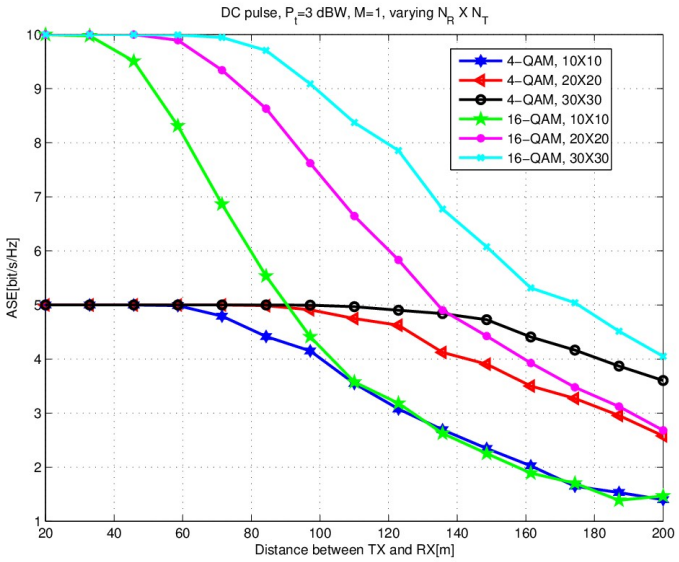

Fig. 9. ASE versus distance; impact of modulation cardinality and array size.

considered, one with time-domain equalization and one with cyclic prefix plus frequency domain equalization. Results have shown that the proposed TDE structure outperforms the FDE, as well as that for distances up to 100m and for values of the transmit power around 0dBW very good performance level can be attained, with ASE values up to 10 bit/s/Hz, which, for a bandwidth of 500MHz, leads toa bit-rate of up to 5Gbit/s. The present study can be generalized and strengthened in many directions. First of all, the impact of hybrid analog/digital beamforming should be evaluated; moreover, the considered analysis might be applied to a point-to-multipoint link, wherein the presence of multiple antennas at the transmitter is used for simultaneous communication with distinct users (the so-called multiuser MIMO technique). Additionally, since, as already discussed, the reduced wavelength of mmWave permits installing arrays with many antennas in small volumes, an analysis, possibly through asymptotic analytic considerations, of the very large number of antennas regime could also be made. Last, but not least, energy-efficiency considerations should also be made: both the ASE and the transceiver power consumption increase for increasing transmit power and increasing size of the antenna arrays; if we focus on the ratio between the ASE and the transceiver power consumption, namely on the system energy efficiency, optimal trade-off values for the transmit power and size of the antenna arrays should be found. These topics are certainly worth future investigation.

REFERENCES

[1] J. G. Andrews, S. Buzzi, W. Choi, S. Hanly, A. Lozano, A. C. Soong, and J. C. Zhang, "What will 5G be?" *IEEE J. Select. Areas Commun.*, vol. 32, no. 6, Jun. 2014.

[2] E. Larsson, O. Edfors, F. Tufvesson, and T. Marzetta, "Massive MIMO for next generation wireless systems," *IEEE Commun. Mag.*, vol. 52, no. 2, pp. 186–195, February 2014.

[3] V. Jungnickel, K. Manolakis, W. Zirwas, B. Panzner, V. Braun, M. Lossow, M. Sternad, R. Apelfro?jd, and T. Svensson, "The role of small cells, coordinated multipoint, and massive MIMO in 5G," *IEEE Commun. Mag.*, vol. 52, no. 5, pp. 44–51, May 2014.

[4] T. S. Rappaport, S. Sun, R. Mayzus, H. Zhao, Y. Azar, K. Wang, G. N. Wong, J. K. Schulz, M. Samimi, and F. Gutierrez, "Millimeter wave mobile communications for 5G cellular: It will work!" *IEEE Access*, vol. 1, pp. 335–349, May 2013.

[5] A. Ghosh, T. A. Thomas, M. Cudak, R. Ratasuk, P. Moorut, F. W. Vook, T. Rappaport, J. G. R MacCartney, S. Sun, and S. Nie, "Millimeter wave enhanced local area systems: A high data rate approach for future wireless networks," *IEEE J. Select. Areas Commun.*, vol. 32, no. 6, pp. 1152 – 1163, Jun. 2014.

[6] T. S. Rappaport, F. Gutierrez, E. Ben-Dor, J. Murdock, Y. Qiao, and J. I. Tamir, "Broadband millimeter-wave propagation measurements and models using adaptive-beam antennas for outdoor urban cellular communications," *IEEE Trans. Antennas and Prop.*, vol. 61, no. 4, pp. 1850–1859, Apr. 2013.

[7] T. Bai, A. Alkhateeb, and R. Heath, "Coverage and capacity of millimeter-wave cellular networks," *IEEE Commun. Mag.*, vol. 52, no. 9, pp. 70–77, September 2014.

[8] A. Alkhateeb, J. Mo, N. Gonzalez-Prelcic, and R. Heath, "MIMO precoding and combining solutions for millimeter-wave systems," *IEEE Commun. Mag.*, vol. 52, no. 12, pp. 122–131, December 2014.

[9] P. Banelli, S. Buzzi, G. Colavolpe, A. Modenini, F. Rusek, and A. Ugolini, "Modulation formats and waveforms for 5G networks: Who will be the heir of OFDM?" *IEEE Signal Processing Mag.*, vol. 31, no. 6, pp. 80–93, Nov. 2014.

[10] L. Deneire, B. Gyselinckx, and M. Engels, "Training sequence versus cyclic prefix-a new look on single carrier communication," *IEEE Communication Letters*, vol. 5, no. 7, pp. 292–294, July 2001.

[11] M. Cudak *et al.*, "Moving towards mmwave-based beyond-4G (b-4G) technology," in *Proc. IEEE 77th VTC Spring*, June 2013.

[12] S. Larew, T. Thomas, M. Cudak, and A. Ghosh, "Air interface design and ray tracing study for 5G millimeter wave communications," in *2013 IEEE Globecom Workshops*, Dec 2013, pp. 117–122.

[13] O. El Ayach, S. Rajagopal, S. Abu-Surra, Z. Pi, and R. Heath, "Spatially sparse precoding in millimeter wave MIMO systems," *IEEE Trans. on Wireless Commun.*, vol. 13, no. 3, pp. 1499–1513, March 2014.

[14] A. Alkhateeb and R. W. Heath, Jr, "Frequency selective hybrid precoding for limited feedback millimeter wave systems," *ArXiv e-prints*, Oct. 2015. [Online]. Available: http://arxiv.org/abs/1510.00609

[15] D. M. Arnold, H.-A. Loeliger, P. O. Vontobel, A. Kavčić, and W. Zeng, "Simulation-based computation of information rates for channels with memory," *IEEE Trans. Inform. Theory*, vol. 52, no. 8, pp. 3498–3508, Aug. 2006.

[16] A. Viholainen, M. Bellanger, and M. Huchard, "Prototype filter and structure optimization," D3.1 of PHYsical layer for DYnamic AccesS and cognitive radio (PHYDYAS), FP7-ICT Future Networks, Tech. Rep., Jan. 2008.

[17] C. Dolph, "A current distribution for broadside arrays which optimizes the relationship between beam width and side-lobe level," *Proceedings of the IRE*, vol. 34, no. 6, pp. 335–348, June 1946.

[18] A. Antoniou, *Digital Filters: Analysis, Design and Applications*. McGraw-Hill, 2000.

[19] M. Abramowitz and I. A. Stegun, Eds., *Handbook of Mathematical Functions*. Dover, 1972.

[20] S. Singh, M. Kulkarni, A. Ghosh, and J. Andrews, "Tractable model for rate in self-backhauled millimeter wave cellular networks," *IEEE J. Select. Areas Commun.*, vol. 33, no. 10, pp. 2196–2211, Oct 2015.